State of Charge Estimation for Lithium-Ion Batteries Based on a Nonlinear Fractional Model

Baojin Wang, Zhiyuan Liu, *Member, IEEE,* Shengbo Eben Li, *Member, IEEE,*
Scott Jason Moura, *Member, IEEE,* and Huei Peng

***Abstract*—This paper presents a new battery state of charge (SOC) estimation method for lithium-ion batteries based on a nonlinear fractional model with incommensurate differentiation orders. A continuous frequency distributed model is used to describe the incommensurate fractional system. A Luenberger-type observer is designed for battery SOC estimation. The observer gain that can stabilize the zero equilibrium of the estimation error system is derived by the Lyapunov's direct method. The proposed SOC observer is examined using real-time experimental data of lithium-ion batteries. The robustness of the observer under different test conditions, including different aging levels, different driving cycles and different cells, is also presented.**

***Index Terms*—Lithium-ion battery, state of charge, incommensurate fractional system, Lyapunov stability, linear matrix inequality.**

I. Introduction

LITHIUM-ION batteries (LIBs) have emerged as the most-promising enabling technology for electrified vehicles. When using LIBs in practical applications, accurate battery state of charge (SOC) estimation is especially important to maintain safe and efficient operation [1]. In addition, accurate SOC estimation enables larger usable energy capacity by reducing uncertainty at the voltage limits, thereby enhancing range.

Accurate and reliable SOC estimation has been a long-standing challenge. Existing studies can be roughly classified into two categories: open-loop and closed-loop methods. The former typically includes ampere-hour counting and open-circuit-voltage (OCV) calibration [2]. The ampere-hour counting method is trivial to implement, but suffers from drift due to current measurement bias and requires a known initial condition [3]. The OCV calibration method requires exact knowledge of OCV as a function of SOC. In practice, the OCV relationship changes over time and temperature. Closed-loop methods can provide improved accuracy compared to their open-loop counterparts, since they are fundamentally robust to modeling and measurement errors. The main idea is to fuse a battery model with measurable signals, i.e., battery voltage, current and temperature, to predict the internal state, i.e., SOC. Accurate battery models are of essential importance for closed-loop methods. Equivalent circuit models (ECMs) have been widely used in SOC estimation due to their intuitive structure and (often, but not always) low computational requirements [4], [5]. One shortcoming of ECMs is that they are unable to accurately characterize the electrochemical dynamics since they mimic the input-output behavior by electric components, e.g., resistors and capacitors. The electrochemical models conquer some shortcomings of ECMs by using coupled and nonlinear partial differential equations (PDEs) [6], [7]. These PDEs describe ion transport phenomena and electrochemical reactions to achieve higher accuracy, but inevitably require advanced numerical implementation methods. Even with the simplest electrochemical models, i.e., the single particle model (SPM) [8], such a SOC estimator can include tens of unknown parameters to be designed.

Impedance-based models are an alternative choice for SOC estimation. A key feature of impedance-based models is they naturally cast themselves into fractional impedance components, e.g., the constant phase element (CPE) and Warburg element [9]. The potential advantages of fractional models has been discussed for accurate representation of battery dynamics [10], [11]. The commonly used ECMs, e.g., the first-order RC and second-order RC models, can be considered as low-order approximations of fractional battery models [12]. In addition, a key advantage of fractional models is they model infinite dimensional systems with only a few parameters [13]. Consequently, fractional models hold interesting advantages for SOC estimation. A pioneering work has been done by Sabatier, et al. (2006), in which a fractional model for lead acid battery is built, and its parameters are identified after approximation in the frequency domain. [14]. A similar fractional model was derived by Xu, et al. (2013), the Kalman filter was applied to estimate battery SOC after approximating the model based on the Grünwald-Letnikov definition [9].

The observer design methods for integer systems have been extended to fractional systems in recent years. For instance, a pole placement-based observer was reported for both commensurate and incommensurate fractional systems [15]. This, however, is not extendable to nonlinear systems. Lyapunov's approach has not been explored until recently. Trigeassou, et al., proposed a method to analyze stability for fractional systems using Lyapunov stability theory [16], where the key

Manuscript received July 16, 2015. This work is supported by China Automobile Industry Innovation and Development Joint Fund (NO. U1564207). *(Corresponding author: Baojin Wang.)*

B. Wang and Z. Liu are with the Department of Control Science and Engineering, Harbin Institute of Technology, Harbin, 150001, China (e-mail: baojin.w@gmail.com; e-mail: liuzy_hit@hit.edu.cn).

S.E. Li is with the State Key Lab of Automotive Safety and Energy, Tshinghua University, Beijing, 150001, China, (e-mail: lisb04@gmail.com).

S.J. Moura is with the Department of Civil & Environmental Engineering, University of California, Berkeley, CA, 94720, USA, (e-mail: scott.moura@gmail.com).

H. Peng is with the Department of Mechanical Engineering, University of Michigan University, Ann Arbor, MI, 48109, USA, (e-mail: hpeng@umich.edu).

is to introduce a continuous frequency distributed model and an appropriate Lyapunov function. Following this concept, Boroujeni and Momeni designed a fractional observer for a class of commensurate nonlinear fractional systems [17]. Lan and Zhou incorporated a positive definite matrix into Boroujeni's Lyapunov function to mitigate conservation for commensurate fractional systems [18]. Consequently, one can prove Lyapunov stability using the framework of linear matrix inequalities (LMIs), which we leverage in this paper. Nevertheless, it is more reasonable to model physical systems with incommensurate fractional equations [13], e.g., the fractional model used for LIBs in this paper, which needs observer design methods applicable to incommensurate fractional system.

The major contribution of this paper is to design an observer for battery SOC estimation using a nonlinear fractional battery model with incommensurate differentiation orders. The observer is designed for the original fractional model, rather than an approximation. We design this observer to be provably stable via Lyapunov theory. The remainder of this paper is organized as follows: Section II introduces the fractional model for LIBs. Section III proposes the novel nonlinear fractional observer for SOC estimation. Section IV introduces the battery tests and realization methods for the fractional systems. Experimental results and discussions are provided in Section V. Conclusions are presented in Section VI.

II. Fractional Model for Batteries

A. Definitions for Fractional Calculus

Fractional calculus, which involves non-integer derivatives and integrals, was first introduced by Leibniz in 1695. It has not attracted significant attention within engineering until recently, where several physical systems were found to be better characterized by non-integer derivatives and integrals [19], [20]. In general, physical systems with mass transport, diffusion dynamics and memory hysteresis can be elegantly described by fractional calculus. One reason for this is that fractional differential equations are a natural mathematical tool to describe distributed-parameter systems [21]. Consequently, fractional calculus is an appropriate tool for characterizing the electrochemical dynamics in batteries.

In fractional calculus, the operator ${}_{t_0}\mathscr{D}_t^q$ is used to represent the derivative or integral of arbitrary order q with respect to t, in which t_0 is the initial time. Here, t_0 is considered as 0 in this paper. When $q > 0$, ${}_{t_0}\mathscr{D}_t^q$ represents the fractional derivative; when $q < 0$, it stands for the fractional integral. In this paper, we consider only fractional derivatives, i.e., $q > 0$, and the operator is then simplified as $\mathscr{D}^q$.

The Grünwald-Letnikov definition is one of the most commonly used definitions [22], [23]. The q-th order Grünwald-Letnikov fractional derivative of $x(t)$ is defined as:

$$\mathscr{D}^q x(t) = \lim_{\Delta T \to 0} \frac{1}{\Delta T^q} \sum_{i=0}^{[t/\Delta T]} (-1)^i \binom{q}{i} x(t - i\Delta T) \quad (1)$$

where ΔT is the sampling time, $[t/\Delta T]$ stands for the integer part of $t/\Delta T$, $\binom{q}{i}$ represents the Newton binomial coefficient generalized to real numbers, expressed as:

$$\binom{q}{i} = \frac{\Gamma(q+1)}{\Gamma(i+1)\,\Gamma(q-i+1)} \quad (2)$$

where $\Gamma(q)$ represents the Gamma function, defined by:

$$\Gamma(q) = \int_0^\infty \xi^{q-1} e^{-\xi} d\xi.$$

The Gamma function plays a very important role in fractional calculus, which is a generalization of the factorial operator for real numbers. In addition, the state-space representation of a linear time-invariant fractional system is similar to that of an integer system:

$$\begin{aligned} \mathscr{D}^\alpha x(t) &= Ax(t) + Bu(t) \\ y(t) &= Cx(t) + Du(t) \end{aligned} \quad (3)$$

where $x(t) \in \mathbb{R}^n$ is the state vector, $u(t) \in \mathbb{R}^r$ is the system input vector, $y(t) \in \mathbb{R}^p$ is the system output vector, A, B, C, and D are the matrices with appropriate dimensions, and $\alpha = \begin{bmatrix} \alpha_1 & \alpha_2 & \dots & \alpha_n \end{bmatrix}$ is the differentiation order vector. Note that, if all the elements of α are the same, i.e., $\alpha_1 = \alpha_2 = \ldots = \alpha_n$, (3) is a commensurate fractional system, otherwise it is incommensurate [22].

For engineering implementation, (3) can be discretized in time based on the Grünwald-Letnikov fractional derivative, for $k \geq 1$:

$$\begin{aligned} x(k+1) = {} & [\Delta T^\alpha A + \operatorname{diag}(\alpha) I]\, x(k) \\ & - \sum_{i=2}^{N+1} (-1)^i \binom{\alpha}{i} x(k+1-i) \\ & + \Delta T^\alpha B u(k) \end{aligned} \quad (4)$$

and for $k = 0$:

$$x(k+1) = [\Delta T^\alpha A + \operatorname{diag}(\alpha) I]\, x(k) + \Delta T^\alpha B u(k). \quad (5)$$

Above are the basic definitions used in this paper.

B. Fractional Modeling with Incommensurate Differentiation Orders

A typical electrochemical impedance spectroscopy (EIS) diagram for LIBs is shown in Fig. 1. For the EIS analysis, fractional elements, e.g., CPE and Warburg element, are frequently used instead of common RC circuits to achieve higher accuracy. The advantage of this replacement has been noticed for some time-domain applications in recent years [10], [11]. Due to the lack of effective techniques, those fractional elements are usually approximated by a series of RC circuits for battery applications, which inevitably introduces a certain level of approximation error. Different from previous studies, this paper presents a method to directly apply a fractional battery model to design robust SOC estimator. A fractional battery model, shown in Fig. 2, is used to describe battery behaviors. This model can be regarded as a variant of the second-order RC model, with two capacitors replaced by two CPEs.

Note that, although the CPE is usually characterized with arbitrary differentiation orders within $[0, 1]$ in the literature,

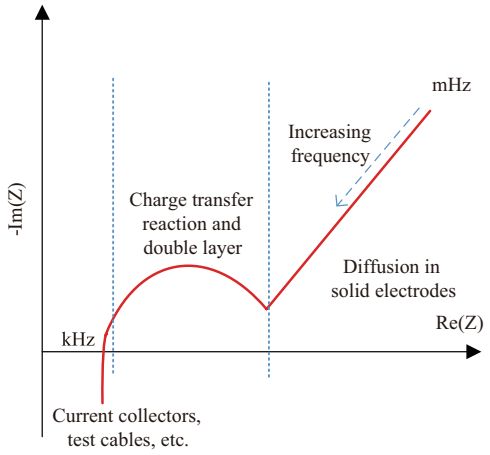

Fig. 1. Typical EIS diagram for LIBs.

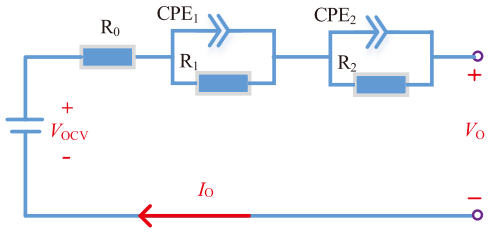

Fig. 2. Fractional battery model structure used in this paper.

the two boundary values are not considered here. Hence, the two differentiation orders are defined in the range of $(0,1)$ in this work. The dynamic equation of a CPE in parallel with a resistor is derived as bellow:

$$\mathscr{D}^{\alpha_i} V_{CPE_i}(t) = -\frac{1}{R_i C_i} V_{CPE_i}(t) + \frac{1}{C_i} I_O(t), i = 1,2 \quad (6)$$

where $V_{CPE_i}(t)$ represents the CPE voltage, $I_O(t)$ is the battery current, R_i and C_i are the element parameters, $\alpha_i \in \mathbb{R}, 0 < \alpha < 1$ is the differentiation order. Another state of the fractional battery model is SOC, usually expressed as:

$$\frac{dSOC(t)}{dt} = -I_O(t)\frac{\eta}{Q_n} \quad (7)$$

where, η is charging/discharging efficiency, Q_n is the nominal battery capacity.

Consequently, the battery is modeled as a nonlinear fractional system with incommensurate differentiation orders. Since the two CPEs are used to represent different dynamics, the two differentiation orders have no connection with each other and are defined as two independent parameters.

The battery can then be expressed by the following state-space representation:

$$\begin{aligned} \mathscr{D}^{\alpha} x(t) &= Ax(t) + Bu(t) \\ y(t) &= Cx(t) + Du(t) + f[x(t)] \end{aligned} \quad (8)$$

where $x(t) = \begin{bmatrix} V_{CPE_1}(t) & V_{CPE_2}(t) & SOC(t) \end{bmatrix}^T$ is the state vector, $y(t)$ is the system output (battery terminal voltage V_O), $u(t)$ represents the system input (battery current I_O), $\alpha = \begin{bmatrix} \alpha_1 & \alpha_2 & 1 \end{bmatrix}$ represents the incommensurate order vector, A, B, C, and D are the matrices with appropriate dimensions:

$$\begin{aligned} A &= \begin{bmatrix} -\frac{1}{R_1 C_1} & 0 & 0 \\ 0 & -\frac{1}{R_2 C_2} & 0 \\ 0 & 0 & 0 \end{bmatrix} \\ B &= \begin{bmatrix} 1/C_1 & 1/C_2 & -\eta/Q_n \end{bmatrix}^T \\ C &= \begin{bmatrix} -1 & -1 & d_1 \end{bmatrix} \\ D &= -R_0 \end{aligned} \quad (9)$$

where, $d_k, k = 0, 1, \cdots, M$ are the coefficients of $f^*[x(t)] = \sum_{k=0}^{M} d_k SOC^k(t)$. The function $f^*[x(t)]$ has been extensively and successfully used to represent the OCV-SOC relationship for many different batteries [4], [24]. The function $f[x(t)]$ in (8) is defined as:

$$f[x(t)] = \sum_{k=0, k\neq 1}^{M} d_k SOC^k(t). \quad (10)$$

In other words, the linear term $d_1 SOC(t)$ is excluded from $f^*[x(t)]$ and incorporated into the input matrix C. For most battery chemistries, it can be easily shown that (10) is Lipschitz continuous within $0 \leq \text{SOC} \leq 1$, i.e.,

$$\|f(SOC_1) - f(SOC_2)\| \leq \gamma \|SOC_1 - SOC_2\| \quad (11)$$

where γ is the Lipschitz constant, provided that $|d_k| < \infty$ for all $k = 0, \cdots, M$ and $M > 0$. Condition (11) is frequently used to deal with Lipschitz nonlinearities, which may lead to unfeasible LMIs when the Lipschitz constant is too large.

The fractional model governed by (8)-(10) includes both integer and fractional states. The two differentiation orders for the CPEs are defined as arbitrary parameters in the range of $(0,1)$ to achieve higher accuracy. However, most existing methods for fractional observer design are applicable to commensurate fractional systems. Our objective is to design an observer for an incommensurate nonlinear fractional system for battery SOC estimation based on the Lyapunov approach.

III. Fractional Observer for SOC Estimation

In this section we design a novel state observer using a continuous frequency distributed model representation of the fractional model, and Lyapunov stability theory. Specifically, sufficient conditions are derived for the stability of an incommensurate nonlinear fractional observer via Lyapunov's direct method.

Considering the fractional battery model defined by (8)-(10), the following observer is proposed:

$$\begin{aligned} \mathscr{D}^{\alpha} \hat{x}(t) &= A\hat{x}(t) + Bu(t) + L[y(t) - \hat{y}(t)] \\ \hat{y}(t) &= C\hat{x}(t) + Du(t) + f[\hat{x}(t)] \end{aligned} \quad (12)$$

where $\hat{x}(t)$ is the state estimation, $\hat{y}(t)$ denotes the output estimation, and L is the observer gain to be designed. The following lemma is used for deriving sufficient conditions for observer stability.

Lemma 1 [16], [25]: A fractional differential equation, $\mathscr{D}^{\alpha_i} x_i(t) = g_i(t)$, is equivalent to the following continuous frequency distributed model, for $0 < \alpha_i < 1$:

$$\begin{aligned} \frac{\partial z_i(\omega,t)}{\partial t} &= -\omega z_i(\omega,t) + g_i(t) \\ x_i(t) &= \int_0^\infty \mu_i(\omega) z_i(\omega,t)\, d\omega \\ \mu_i(\omega) &= \frac{\sin(\alpha_i \pi)}{\pi} \omega^{-\alpha_i} \end{aligned} \tag{13}$$

and for $\alpha_i = 1$, $\mathscr{D}^{\alpha_i} x_i(t) = g_i(t)$ can be represented as:

$$\begin{aligned} \frac{\partial z_i(\omega,t)}{\partial t} &= -\omega z_i(\omega,t) + g_i(t) \\ x_i(t) &= \int_0^\infty \mu_i(\omega) z_i(\omega,t)\, d\omega \\ \mu_i(\omega) &= \delta(\omega) \end{aligned} \tag{14}$$

where $g_i(t)$ represents the input, and $x_i(t)$ denotes the output, $z_i(\omega,t)$ is the frequency distributed state variable, $\mu_i(\omega)$ is the frequency weighting function. Interested readers may refer to [16], [25] for additional details.

It should be noted that a fractional differential equation can be exactly converted into a continuous frequency distributed state model by *Lemma 1*. In addition, $x_i(t)$ is the weighted summation of the frequency distributed state variables $z_i(\omega,t)$, where ω is defined in the range of $[0,\infty)$. Therefore we have a continuum of frequency distributed state variables, e.g., $z_i(\omega_1,t)$, $z_i(\omega_2,t)$, $\cdots$, in other words, $z_i(\omega,t)$ is the true state variable. This is also the basis for defining a Lyapunov function for the fractional system described by a continuous frequency distributed model.

The following theorem provides sufficient conditions for the zero equilibrium of the estimation error dynamics.

Theorem 1: Consider the following error dynamics associated with fractional observer (12):

$$\mathscr{D}^{\alpha} \tilde{x}(t) = A_{cl}\tilde{x}(t) + LF(t) \tag{15}$$

where $\tilde{x}(t) = x(t) - \hat{x}(t)$, L is the observer gain, $A_{cl} = A - LC$, $F(t) = f[\hat{x}(t)] - f[x(t)]$. The zero equilibrium is globally asymptotically stable, if there exists a positive definite diagonal matrix P and a scalar $\varepsilon > 0$, together with a matrix L_0 of appropriate dimensions, such that:

$$\begin{bmatrix} A^TP + PA - L_0C - C^TL_0^T + \varepsilon\gamma^2 I & L_0 \\ L_0^T & -\varepsilon \end{bmatrix} < 0 \tag{16}$$

where $L_0 = PL$, and the observer gain can be derived by $L = P^{-1}L_0$.

Proof: The observer error dynamics (15) usually cannot be directly analyzed with Lyapunov theory, as is the case for its integer counterpart. According to *Lemma 1*, (15) can be exactly converted into:

$$\begin{aligned} \frac{\partial z(\omega,t)}{\partial t} &= -\omega z(\omega,t) + A_{cl}\tilde{x}(t) + LF(t) \\ \tilde{x}(t) &= \int_0^\infty \mu(\omega) z(\omega,t)\, d\omega \end{aligned} \tag{17}$$

where:

$$\begin{aligned} z(\omega,t) &= \begin{bmatrix} z_1(\omega,t) & z_2(\omega,t) & z_3(\omega,t) \end{bmatrix}^T \\ \tilde{x}(t) &= \begin{bmatrix} \tilde{V}_{CPE_1}(t) & \tilde{V}_{CPE_2}(t) & \widetilde{SOC}(t) \end{bmatrix}^T \\ \mu(\omega) &= \mathrm{diag}\begin{bmatrix} \mu_1(\omega) & \mu_2(\omega) & \mu_3(\omega) \end{bmatrix} \\ &= \begin{bmatrix} \frac{\sin(\alpha_1\pi)}{\pi}\omega^{-\alpha_1} & 0 & 0 \\ 0 & \frac{\sin(\alpha_2\pi)}{\pi}\omega^{-\alpha_2} & 0 \\ 0 & 0 & \delta(\omega) \end{bmatrix}. \end{aligned}$$

Let us define a Lyapunov function:

$$V(t) = \int_0^\infty v(\omega,t)\, d\omega \tag{18}$$

where $v(\omega,t) = z^T(\omega,t)\,\mu^T(\omega)\,Pz(\omega,t)$ is a monochromatic function with respect to elementary frequency ω, and P is a positive diagonal matrix. It can be seen that the Lyapunov function, $V(t)$, is the summation of all the monochromatic functions $v(\omega,t)$ in the frequency domain.

Theoretically, the zero equilibrium of the error dynamics (15) is globally asymptotically stable if $V(t)$ is positive definite and its time derivative is negative definite. Lyapunov functional $V(t)$ can be expanded as:

$$\begin{aligned} V(t) = \int_0^\infty \big[& p_1\mu_1(\omega) z_1^2(\omega,t) + p_2\mu_2(\omega) z_2^2(\omega,t) \\ & + p_3\mu_3(\omega) z_3^2(\omega,t) \big]\, d\omega \end{aligned} \tag{19}$$

where p_1, p_2 and p_3 are the scalar diagonal elements of P. Note that in the third term on the right side of (19), $\mu_3(\omega) = \delta(\omega)$, then we have:

$$\int_0^\infty \delta(\omega) z_3^2(\omega,t)\, d\omega = z_3^2(0,t). \tag{20}$$

As a result, (19) is equal to:

$$\begin{aligned} V(t) = \int_0^\infty & \big[p_1\mu_1(\omega) z_1^2(\omega,t) + p_2\mu_2(\omega) z_2^2(\omega,t) \big]\, d\omega \\ & + p_3 z_3^2(0,t). \end{aligned} \tag{21}$$

In (21), p_1, p_2 and p_3 are always positive, and thus $V(t)$ is positive definite.

In the following, we will prove that the proposed observer gain ensures $\dot{V}(t) < 0$. The derivative of $V(t)$ takes the form of (22). Note that the term $\mu^T(\omega)\,P$ in (22) obeys the commutative law of multiplication, i.e., $\mu^T(\omega)P = P\mu^T(\omega)$, using the assumption that P is positive definite and diagonal. As a result, (22) is simplified to:

$$\begin{aligned} \dot{V}(t) = & -2\int_0^\infty \omega z^T(\omega,t)\,\mu^T(\omega)\,Pz(\omega,t)\, d\omega \\ & + 2\tilde{x}^T(t) A_{cl}^T P\tilde{x}(t) + 2\tilde{x}^T(t) L_0 F(t). \end{aligned} \tag{23}$$

Note that $\int_0^\infty \omega z^T(\omega,t)\,\mu^T(\omega)\,Pz(\omega,t)\, d\omega$ is nonnegative, and thus $\dot{V}(t) < 0$ can be ensured if the following inequality holds:

$$\tilde{x}^T(t)\left(PA_{cl} + A_{cl}^T P\right)\tilde{x}(t) + 2\tilde{x}^T(t) L_0 F(t) < 0. \tag{24}$$

$$\begin{aligned}\dot{V}(t) &= \int_0^\infty z^T(\omega,t)\,\mu^T(\omega)\,P\left[-\omega z(\omega,t)+A_{cl}\tilde{x}(t)+LF(t)\right]d\omega \\ &\quad+\int_0^\infty \left[-\omega z(\omega,t)+A_{cl}\tilde{x}(t)+LF(t)\right]^T\mu^T(\omega)\,Pz(\omega,t)d\omega \\ &= -2\int_0^\infty \omega z^T(\omega,t)\,\mu^T(\omega)\,Pzd\omega+\int_0^\infty z^T(\omega,t)\,\mu^T(\omega)\,PA_{cl}\tilde{x}(t)\,d\omega+\int_0^\infty z^T(\omega,t)\,\mu^T(\omega)\,L_0F(t)\,d\omega \\ &\quad+\int_0^\infty \tilde{x}^T(t)\,A_{cl}^T\mu^T(\omega)Pz(\omega,t)\,d\omega+\int_0^\infty F^T(t)\,L^T\mu^T(\omega)Pz(\omega,t)\,d\omega\end{aligned} \tag{22}$$

To simplify inequality (24), apply Youngs inequality [26], giving:

$$\begin{aligned}&\tilde{x}^T(t)\left(PA_{cl}+A_{cl}^TP\right)\tilde{x}(t)+2\tilde{x}^T(t)\,L_0F(t) \\ &\le \tilde{x}^T(t)\left(PA_{cl}+A_{cl}^TP\right)\tilde{x}(t) \\ &\quad+\left[\frac{1}{\varepsilon}\tilde{x}^T(t)\,L_0L_0^T\tilde{x}(t)+\varepsilon F^T(t)\,F(t)\right].\end{aligned} \tag{25}$$

Substituting inequality (11) into (25), concludes that:

$$\begin{aligned}&\tilde{x}^T(t)\left(PA_{cl}+A_{cl}^TP\right)\tilde{x}(t) \\ &\quad+\left[\frac{1}{\varepsilon}\tilde{x}^T(t)\,L_0L_0^T\tilde{x}(t)+\varepsilon F^T(t)\,F(t)\right] \\ &\le \tilde{x}^T(t)\left(PA_{cl}+A_{cl}^TP\right)\tilde{x}(t) \\ &\quad+\frac{1}{\varepsilon}\tilde{x}^T(t)\,L_0L_0^T\tilde{x}(t)+\varepsilon\gamma^2\tilde{x}^T(t)\,\tilde{x}(t)\end{aligned} \tag{26}$$

and thus if inequality (27) holds, $\dot{V}(t)<0$ can be guaranteed.

$$A^TP+PA-L_0C-C^TL_0^T+\frac{1}{\varepsilon}L_0L_0^T+\varepsilon\gamma^2I<0. \tag{27}$$

Equation (27) can be converted into the following LMI based on the Schur complement:

$$\begin{bmatrix} A^TP+PA-L_0C-C^TL_0^T+\varepsilon\gamma^2I & L_0 \\ L_0^T & -\varepsilon \end{bmatrix}<0. \tag{28}$$

Consequently, $\dot{V}(t)<0$ is verified if LMI (28) holds, which completes the proof. ■

IV. Model Identification and Observer Realization

In this section, we introduce the experimental battery tests, time domain parameter identification, and numerical implementation of the SOC observer.

A. Battery Tests and Parameter Identification

Eight cylindrical lithium-ion cells are tested and used for verification. The battery cell model is UR14650P from Sanyo.

The experimental setup is provided in Fig. 3. The test instruments include an Arbin BT2000 tester for voltammetric measurement, a thermal chamber for environmental control, a computer for user-machine interface, a switching board for cable connection, and a cell tray for testing insider the chamber. Both current and voltage are recorded at 8 Hz, and therefore the sampling time is $\Delta T=0.125\ s$. The cells are tested under three different test cycles, including a Dynamic

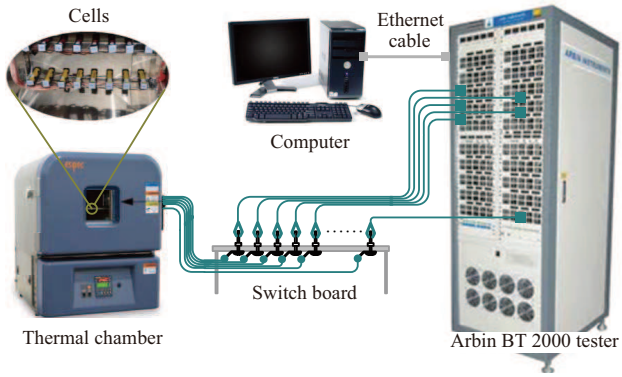

Fig. 3. Battery test setup.

Stress Test (DST), a Federal Urban Dynamic Schedule (FUDS) and a Hybrid Pulse Power Characterization (HPPC). One of the FUDS datasets for an arbitrarily selected cell under $35\,^oC$ is used for parametric identification. We refer to this data as the "training" dataset.

Evolutionary algorithms, e.g., the hybrid multi-swarm particle swarm optimization (HMPSO) and genetic algorithm, have been previously applied to identify fractional model parameters including differentiation orders [27]. In this paper, the parameters of the resistor and two CPEs, as well as coefficients of the OCV-SOC polynomial are identified using HMPSO for the training dataset and listed in Tables I and II, respectively.

TABLE I
Identified Parameters for Resistors and CPEs

R_0	R_1	C_1	R_2	C_2	α_1	α_2
0.0932	1.0157	615.93	0.2840	157.18	0.4218	0.4399

TABLE II
Identified Coefficients for the OCV-SOC Polynomial

d_0	d_1	d_2	d_3	d_4
3.6064	1.2264	-3.5299	5.4483	-2.6775

Fig. 4 illustrates the model accuracy by comparing the identified results with the training dataset. The root-mean-square error (RMSE) in voltage is 4.98 mV. Consequently, the identified fractional model accurately captures the battery dynamics.

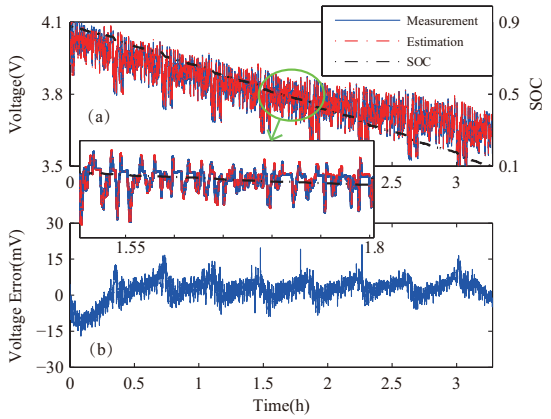

Fig. 4. Model validation using training dataset. (a) Estimated battery voltage vs. measured battery voltage. (b) Estimated battery voltage error.

B. Observer Realization

Numerical techniques are critical for fractional system implementation, and the key is to approximate the fractional derivatives by a series of integer derivatives and/or special functions of the states. For instance, Taylor series expansion is employed in [28] to approximate fractional differential equations. Atanackovic and Stankovic proposed a method that uses the first derivative only to reduce computational burden [29]. The Oustaloup recursive approximation is an alternative approach, and has been widely used to approximate fractional-order transfer functions as integer-order transfer functions [30]. This paper employs the Grünwald-Letnikov fractional derivative in (4) and (5), which is the most straightforward method for numerical implementation. For instance, when $k \geq 1$, the SOC observer (12) is approximated by:

$$\begin{aligned} \hat{x}(k+1) &= \left[\Delta T^{\alpha} A + \operatorname{diag}(\alpha) I\right] \hat{x}(k) \\ &\quad - \sum_{i=2}^{N+1} (-1)^{i} \begin{pmatrix} \alpha \\ i \end{pmatrix} \hat{x}(k+1-i) \\ &\quad + \Delta T^{\alpha} B u(k) + \Delta T^{\alpha} L\left[y(k) - \hat{y}(k)\right] \\ \hat{y}(k) &= C\hat{x}(k) + Du(k) + f(\hat{x}(k)) \end{aligned} \tag{29}$$

where:

$$\Delta T^{\alpha} = \operatorname{diag}\begin{bmatrix} \Delta T^{\alpha_1} & \Delta T^{\alpha_2} & \Delta T \end{bmatrix}$$
$$\begin{pmatrix} \alpha \\ i \end{pmatrix} = \operatorname{diag}\left[\begin{pmatrix} \alpha_1 \\ i \end{pmatrix} \begin{pmatrix} \alpha_2 \\ i \end{pmatrix} \begin{pmatrix} 1 \\ i \end{pmatrix} \right].$$

Theoretically, in (29), the entire past history of state estimates should be involved. This is impractical in real applications where microcontrollers have finite memory limits. Therefore, we truncate past data, which is justified by the short memory principle proposed by Podlubny [31].

V. Estimation Results and Discussions

This section provides SOC estimation results and discussion for different datasets. These datasets include different cells, various test cycles and aging levels.

A. Main Results

The proposed observer design involves the selection of several critical parameters and matrices. The lower bound of the Lipschitz constant γ can be calculated based on (10) and (11), which gives 0.937 in the SOC range of $[0.1, 0.9]$. The parameter γ is selected to be 0.94 in our case, and this is determined by balancing convergence rate and steady-state error fluctuation. Therefore, the LMIs can be solved using the LMI Toolbox in MATLAB:

$$\begin{aligned} \varepsilon &= 5.4914 \times 10^{5} \\ P &= \begin{bmatrix} 5.0729 & 0 & 0 \\ 0 & 2.4231 & 0 \\ 0 & 0 & 1.4951 \end{bmatrix} \times 10^{8} \\ L &= \begin{bmatrix} -1.0135 & -2.0827 & 4.3176 \end{bmatrix}^{T} \times 10^{-3} \end{aligned} \tag{30}$$

The initial estimated state vector is selected to be $\hat{x}(0) = \begin{bmatrix} 0 & 0 & 0.8 \end{bmatrix}^{T}$, while the true SOC is initialized at 0.9. Since the datasets are measured by the Arbin BT2000 tester with high accuracy, the reference SOC curve is calculated based on the ampere-hour counting method with the original datasets. As for the observer, zero mean Gaussian noises are added to the measured current (variance is $0.0004\ \mathrm{A}^2$) and voltage (variance is $0.005\ \mathrm{V}^2$), respectively. In addition, the sampling rate for the observer is set to 1 Hz. In this study, the parameter N for (29) is selected to be 1625 to achieve high accuracy.

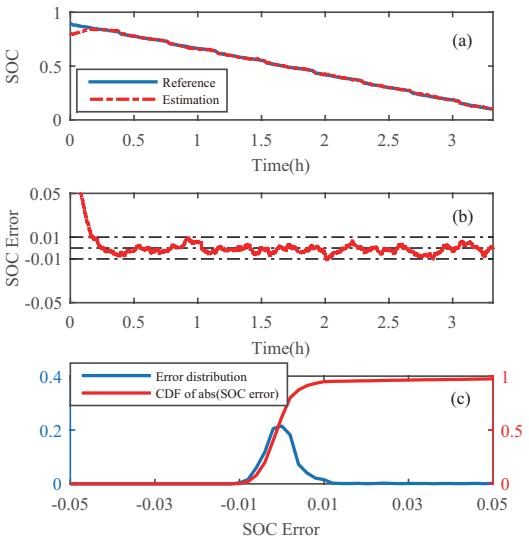

Fig. 5. SOC estimation results for the FUDS reference dataset, $\widehat{SOC}(0) = 0.8$. (a) Estimated SOC vs. measured SOC. (b) SOC estimation error. (c) SOC estimation error distribution and CDF of SOC error.

Fig. 5 shows the SOC estimation results. It can be seen that the proposed observer accurately estimates SOC, and the SOC error is limited within a very narrow error bound, i.e., less than ± 0.01 after convergence. The cumulative distribution function (CDF) of the absolute of SOC error also demonstrates that the estimation error mainly distributes between -0.01 and 0.01. This is essentially related to accurately modeling battery terminal voltage, which is used to correct the estimated SOC.

To further illustrate the observer effectiveness, another simulation is conducted as shown in Fig. 6. Here, the true initial SOC is fixed at 0.9, and the estimated SOC is initialized at

0.3 (In practice, the initial error cannot be so much). Even though the convergence rate is slowed down because the initial estimated SOC is far away from the true value, the estimated SOC finally converges to the true value and then fluctuates in a narrow range.

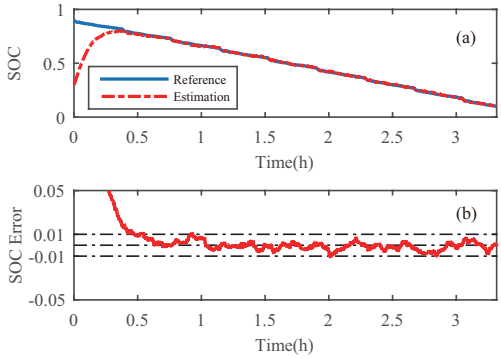

Fig. 6. SOC estimation results for the FUDS reference dataset, $\widehat{SOC}(0) = 0.3$. (a) Estimated SOC vs. measured SOC. (b) SOC estimation error.

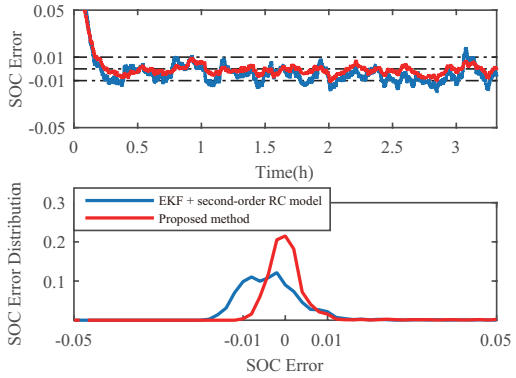

Fig. 7. SOC estimation comparison between EKF + second-order RC model and the proposed method, $\widehat{SOC}(0) = 0.8$.

The frequently used second-order RC model, together with the aforementioned polynomial for OCV-SOC relationship, is employed for comparison. The second-order RC model is calibrated with the same reference dataset, of which the RMSE in voltage is 8.17 mV. In addition, the extended Kalman filter (EKF) is applied for SOC estimation, which is well tuned with similar convergence rate as the proposed method. The comparison can be seen in Fig. 7, illustrating the improved accuracy of the proposed method. The RMS of SOC estimation error for EKF is 8.04×10^{-3}, while that of the proposed method is 3.60×10^{-3}.

The estimation error convergence is related to the Lipschitz constant of the OCV-SOC relationship. Fig. 8 illustrates the SOC estimation errors with different Lipschitz constants. It can be seen that smaller Lipschitz constants accelerate convergence at the expense of noise attenuation. This can help to find the desired observer gain in practice.

B. Robustness Analyses of SOC Estimation

To investigate the robustness of the proposed method, additional numerical tests are performed in this section. In

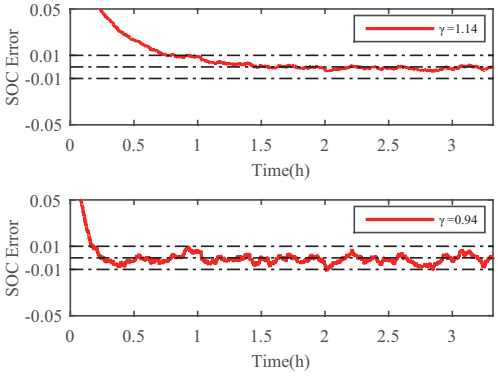

Fig. 8. SOC estimation error with different Lipschitz constants.

the following, the model parameters, listed in Tables I and II, and the observer gain given by (30), are fixed and applied to datasets measured under different test conditions.

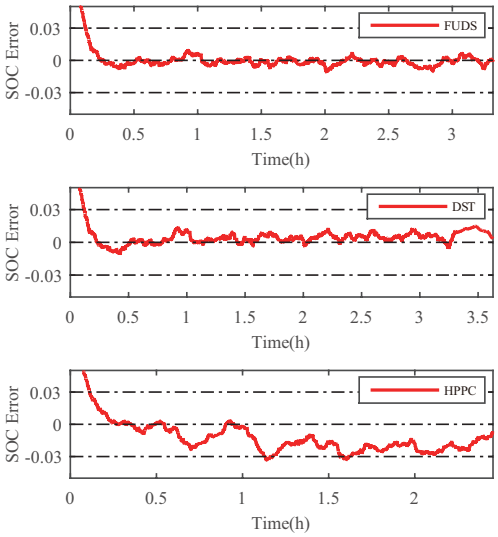

Fig. 9. SOC estimation errors for different test cycles.

We first consider the datasets from different test cycles, i.e., FUDS, DST and HPPC, which have been widely used for battery related studies. Fig. 9 illustrates the SOC estimation results for these three test cycles. The DST dataset produces similar results to FUDS, Nevertheless, the SOC estimation accuracy for HPPC decreases, but remains in the range of $\pm$ 0.03. This can be explained by Fig. 10. The DST and FUDS cycles have similar frequency content, while the HPPC has significant low frequency content. Another reason can be attributed to the different C-rates of the three test cycles. The FUDS and DST have similar average C-rates, while that of the HPPC is different. This is a common shortcoming for models that neglect the influence of C-rate to maintain simple equations.

Battery aging issues are critical for electric vehicles [32], since aged cells exhibit significant parameter variation compared to fresh cells. Consequently, it is necessary to evaluate the SOC estimation performance applied to aged cells. We use the datasets measured from Cycles 300 (reference cycle), 500,

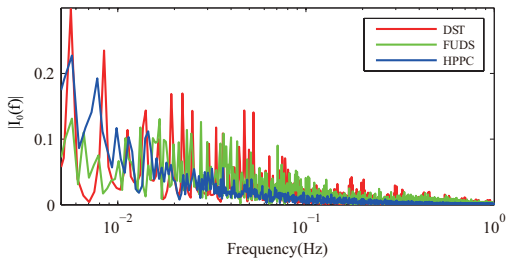

Fig. 10. FFT results of the three test signals (current).

700 and 900 of the reference cell to assess SOC estimation performance (shown in Fig. 11). It can be seen that the estimation performance deteriorates as the cell ages. However, the SOC estimation error remains in the range of $\pm$ 0.03 after 400 aging cycles. The SOC estimation error evolves outside the $\pm$ 0.03 bounds at Cycle 900, illustrating the limitations of the proposed observer and motivating simultaneous state/parameter estimation methods such as [33].

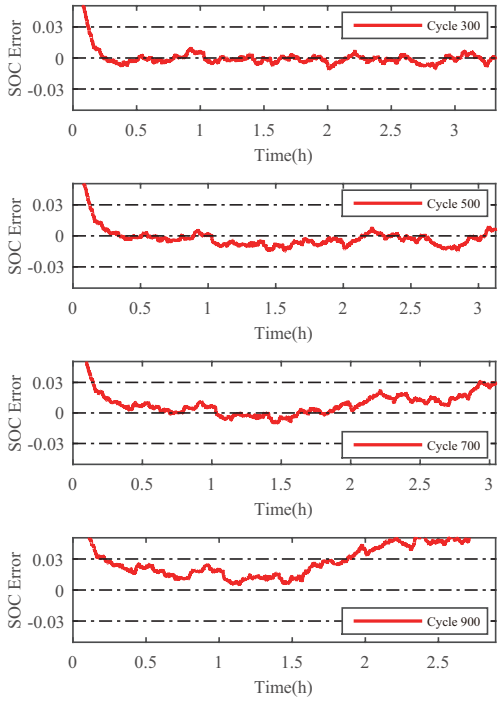

Fig. 11. SOC estimation errors for different aging cycles.

Fig. 12 shows how the SOC estimation error varies for different cells with the same chemistry and same cycle count, illustrating robustness across cells of the same model and cycle count. There is little variation in SOC estimation accuracy across these cells.

VI. Conclusion

This paper presents a novel battery SOC estimation method for lithium ion batteries based on a nonlinear fractional model with incommensurate differentiation orders. A Luenberger-type observer is designed for the SOC estimation. We prove global asymptotic stability of the zero equilibrium of the

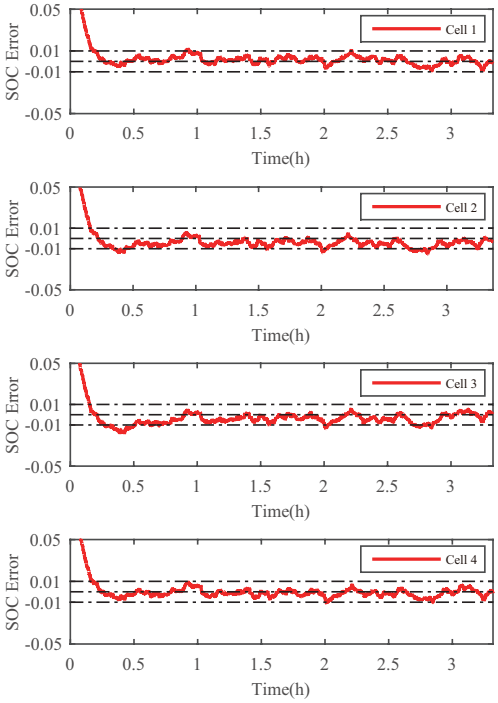

Fig. 12. SOC estimation errors for different cells.

estimation error system using the Lyapunov's direct method. Experimental and simulation results illustrate how the fractional model and observer accurately predict battery dynamics. The robustness of this observer under different test conditions is also discussed.

References

[1] N. A. Chaturvedi, R. Klein, J. Christensen, J. Ahmed, and A. Kojic, "Algorithms for advanced battery-management systems," *IEEE Control Syst.*, vol. 30, no. 3, pp. 49–68, Jun. 2010.

[2] M. Verbrugge and E. Tate, "Adaptive state of charge algorithm for nickel metal hydride batteries including hysteresis phenomena," *J. Power Sources*, vol. 126, no. 12, pp. 236–249, Feb. 2004.

[3] X. Hu, S. Li, H. Peng, and F. Sun, "Robustness analysis of state-of-charge estimation methods for two types of li-ion batteries," *J. Power Sources*, vol. 217, no. 0, pp. 209–219, Nov. 2012.

[4] X. Hu, S. Li, and H. Peng, "A comparative study of equivalent circuit models for li-ion batteries," *J. Power Sources*, vol. 198, no. 0, pp. 359–367, Jan. 2012.

[5] Y. Wang, H. Fang, Z. Sahinoglu, T. Wada, and S. Hara, "Adaptive estimation of the state of charge for lithium-ion batteries: Nonlinear geometric observer approach," *IEEE Trans. Control Syst. Technol,*, vol. 23, no. 3, pp. 948–962, May 2015.

[6] V. Ramadesigan, P. W. C. Northrop, S. De, S. Santhanagopalan, R. D. Braatz, and V. R. Subramanian, "Modeling and simulation of lithium-ion batteries from a systems engineering perspective," *J. Electrochem. Soc.*, vol. 159, no. 3, pp. R31–R45, 2012.

[7] M. Corno, N. Bhatt, S. M. Savaresi, and M. Verhaegen, "Electrochemical model-based state of charge estimation for li-ion cells," *IEEE Trans. Control Syst. Technol,*, vol. 23, no. 1, pp. 117–127, Jan. 2015.

[8] S. Moura, N. Chaturvedi, and M. Krstic, "Pde estimation techniques for advanced battery management systems–part 1: Soc estimation," in *Proc. ACC*, Montreal, QC, Canada, Jun. 2012, pp. 559–565.

[9] J. Xu, C. C. Mi, B. Cao, and J. Cao, "A new method to estimate the state of charge of lithium-ion batteries based on the battery impedance model," *J. Power Sources*, vol. 233, no. 0, pp. 277–284, Jul. 2013.

[10] D. V. Do, C. Forgez, K. El, Kadri Benkara, and G. Friedrich, "Impedance observer for a li-ion battery using kalman filter," *IEEE Transactions on Vehicular Technology*, vol. 58, no. 8, pp. 3930–3937, 2009.

[11] W. Waag and D. U. Sauer, "Adaptive estimation of the electromotive force of the lithium-ion battery after current interruption for an accurate state-of-charge and capacity determination," *Applied Energy*, vol. 111, no. 4, pp. 416–427A, 2013.
[12] B. Wang, S. E. Li, H. Peng, and Z. Liu, "Fractional-order modeling and parameter identification for lithium-ion batteries," *J. Power Sources*, vol. 293, no. 0, pp. 151–161, Oct. 2015.
[13] S. Victor, R. Malti, H. Garnier, and A. Oustaloup, "Parameter and differentiation order estimation in fractional models," *Automatica*, vol. 49, no. 4, pp. 926–935, Apr. 2013.
[14] J. Sabatier, M. Aoun, A. Oustaloup, G. Grgoire, F. Ragot, and P. Roy, "Fractional system identification for lead acid battery sate charge estimation," *Signal Processing*, vol. 86, no. 10, pp. 2645–2657, 2006.
[15] D. M. Senejohnny and H. Delavari, "Linear estimator for fractional systems," *Signal Image Video Process.*, vol. 8, no. 2, pp. 389–396, Feb. 2014.
[16] J.-C. Trigeassou, N. Maamri, J. Sabatier, and A. Oustaloup, "A lyapunov approach to the stability of fractional differential equations," *Signal Process.*, vol. 91, no. 3, pp. 437–445, Mar. 2011.
[17] E. A. Boroujeni and H. R. Momeni, "Non-fragile nonlinear fractional order observer design for a class of nonlinear fractional order systems," *Signal Process.*, vol. 92, no. 10, pp. 2365–2370, Oct. 2012.
[18] Y.-H. Lan and Y. Zhou, "Non-fragile observer-based robust control for a class of fractional-order nonlinear systems," *Syst. Control Lett.*, vol. 62, no. 12, pp. 1143–1150, Dec. 2013.
[19] W. Yu, Y. Luo, and Y. G. Pi, "Fractional order modeling and control for permanent magnet synchronous motor velocity servo system," *Mechatronics*, vol. 23, no. 7, pp. 813–820, Oct. 2013.
[20] A. Narang, S. L. Shah, and T. Chen, "Continuous-time model identification of fractional-order models with time delays," *IET Contr. Theory Appl.*, vol. 5, no. 7, pp. 900–912, May 2011.
[21] C. B. Ma and Y. Hori, "Fractional-order control: Theory and applications in motion control," *IEEE Ind. Electron. Mag.*, vol. 1, no. 4, pp. 6–16, 2007.
[22] I. Petras, *Fractional-order nonlinear systems: modeling, analysis and simulation*. Springer, 2011.
[23] C. A. Monje, Y. Chen, B. M. Vinagre, D. Xue, and V. Feliu, *Fractional-order Systems and Controls: Fundamentals and Applications*. New York: Springer, 2010.
[24] B. Pattipati, B. Balasingam, G. V. Avvari, K. R. Pattipati, and Y. Bar-Shalom, "Open circuit voltage characterization of lithium-ion batteries," *Journal of Power Sources*, vol. 269, no. 3, pp. 317–333, 2014.
[25] J.-C. Trigeassou, N. Maamri, J. Sabatier, and A. Oustaloup, "State variables and transients of fractional order differential systems," *Comput. Math. Appl.*, vol. 64, no. 10, pp. 3117–3140, Nov. 2012.
[26] F. Chen and W. Zhang, "Lmi criteria for robust chaos synchronization of a class of chaotic systems," *Nonlinear Anal.-Theory Methods Appl.*, vol. 67, no. 12, pp. 3384–3393, Dec. 2007.
[27] S. E. Li, B. Wang, H. Peng, and X. Hu, "An electrochemistry-based impedance model for lithium-ion batteries," *J. Power Sources*, vol. 258, no. 0, pp. 9–18, Jul. 2014.
[28] S. Pooseh, R. Almeida, and D. F. M. Torres, "Fractional order optimal control problems with free terminal time," *J. Ind. Manag. Optim.*, vol. 10, no. 2, pp. 363–381, Apr. 2014.
[29] T. M. Atanackovic and B. Stankovic, "On a numerical scheme for solving differential equations of fractional order," *Mech. Res. Commun.*, vol. 35, no. 7, pp. 429–438, Oct. 2008.
[30] A. Oustaloup, X. Moreau, and M. Nouillant, "The crone suspension," *Control Eng. Pract.*, vol. 4, no. 8, pp. 1101–1108, Aug. 1996.
[31] I. Podlubny, *Fractional differential equations: an introduction to fractional derivatives, fractional differential equations, to methods of their solution and some of their applications*. Academic press, 1998, vol. 198.
[32] S. J. Moura, J. L. Stein, and H. K. Fathy, "Battery-health conscious power managementin plug-in hybrid electric vehicles via electrochemical modeling and stochastic control," *IEEE Trans. Control Syst. Technol,*, vol. PP, no. 99, pp. 1–1, May 2013.
[33] S. J. Moura, N. A. Chaturvedi, and M. Krstic, "Adaptive partial differential equation observer for battery state-of-charge/state-of-health estimation via an electrochemical model," *J. Dyn. Syst.-t. Asme.*, vol. 136, no. 1, Jan. 2014.